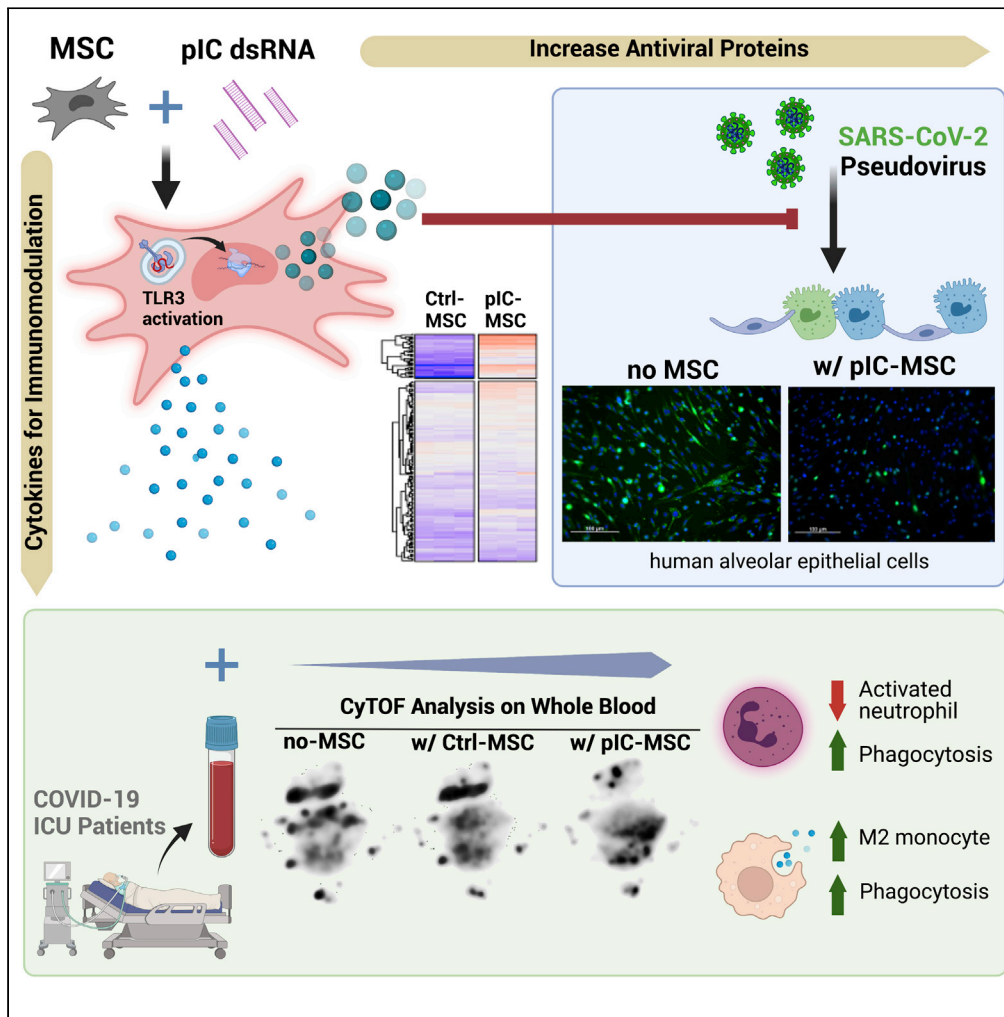


Article

Poly(I:C) enhances mesenchymal stem cell control of myeloid cells from COVID-19 patients



Luciana Souza-Moreira, Yuan Tan, Yan Wang, ..., Shane English, Duncan J. Stewart, Shirley H.J. Mei

smei@ohri.ca

Highlights

Viral stimuli mimic enhances MSC's antiviral and immunomodulatory molecular profile

pIC-primed MSCs inhibit SARS-CoV2 pseudovirus entry into epithelial cells

pIC-MSCs recalibrate dysregulated cellular response in COVID-19 patient's whole blood



Article

Poly(I:C) enhances mesenchymal stem cell control of myeloid cells from COVID-19 patients

Luciana Souza-Moreira,^{1,5} Yuan Tan,^{1,2,5} Yan Wang,¹ Jia-Pey Wang,¹ Mahmoud Salkhordeh,¹ Jennifer Virgo,¹ Maria Florian,¹ Aidan B.P. Murray,¹ Irene Watpool,³ Lauralyn McIntyre,^{2,3,4} Shane English,^{3,4} Duncan J. Stewart,^{1,2} and Shirley H.J. Mei^{1,6,*}

SUMMARY

Mesenchymal stem cells (MSCs) are being studied for the treatment of COVID-19-associated critical illness, due to their immunomodulatory properties. Here, we hypothesized that viral mimic-priming improves MSCs' abilities to rebalance the dysregulated immune responses in COVID-19. Transcriptome analysis of poly(I:C)-primed MSCs (pIC-MSCs) showed upregulation of pathways in antiviral and immunomodulatory responses. Together with increased expression of antiviral proteins such as MX1, IFITM3, and OAS1, these changes translated to greater effector functions in regulating monocytes and granulocytes while further enhancing MSCs' ability to block SARS-CoV-2 pseudovirus entry into epithelial cells. Most importantly, the addition of pIC-MSCs to COVID-19 patient whole blood significantly reduced inflammatory neutrophils and increased M2 monocytes while enhancing their phagocytic effector function. We reveal for the first time that MSCs can be primed by Toll-like receptor 3 agonist to improve their ability to rebalance the dysregulated immune responses seen in severe SARS-CoV-2 infection.

INTRODUCTION

The coronavirus disease 2019 (COVID-19), caused by a novel coronavirus SARS-CoV-2, was declared a pandemic by the WHO in 2020. Severe illness and even death associated with COVID-19 are primarily related to the patients who develop acute respiratory distress syndrome (ARDS), sepsis, and/or multiorgan failure, resulting from dysfunctional immune, endothelial, and coagulation responses triggered by viral infection (Yang et al., 2020). Although monoclonal antibody therapy has shown to be effective yet transiently protective against early SARS-CoV-2 infection, they are only available to those who are not severely ill (Bruzzei et al., 2021). Given the lack of specific treatment for severely ill patients once they are in the intensive care unit (ICU), mesenchymal stem/stromal cells (MSCs) have been investigated in clinical trials as a potential treatment for severe COVID-19 (Leng et al., 2020; Metcalfe, 2020), with currently more than 96 trials registered on clinicaltrials.org.

Currently, there are over 1,200 registered clinical trials studying MSCs in a variety of inflammatory diseases, including but not limited to graft-versus-host disease, rheumatoid arthritis, colitis, and sepsis (McIntyre et al., 2018; Squillaro et al., 2016; Ringdén et al., 2006). Leng et al. was the first to report improved pulmonary function in COVID-19 patients who received MSCs (Leng et al., 2020). A recent double-blind, randomized controlled trial also showed that MSC treatment was safe, improved survival, and shortened time to recovery in COVID-19 patients (Lanzoni et al., 2021). In addition to the above-mentioned trials using MSCs in COVID ARDS, there are other trials that examined the safety and efficacy of MSCs in patients with non-COVID ARDS, most notably the START trial that also demonstrated the safety of administration of MSCs (Matthay et al., 2019; Bellingan et al., 2022). Although the results from these early trials are consistent with the known ability of MSCs to dampen hyperinflammatory response, it is not known how MSCs modulate host immune responses in COVID-19 and whether more can be done to improve MSC therapies.

We hypothesized that double-stranded RNA (dsRNA [viral mimic])-primed MSCs, compared with unprimed MSCs, can improve and more efficiently rebalance the dysregulated immune system associated with viral

¹Regenerative Medicine Program, Ottawa Hospital Research Institute, Ottawa K1H 8L6, ON, Canada

²Faculty of Medicine, University of Ottawa, Ottawa, ON K1H 8L1, Canada

³Critical Care, The Ottawa Hospital, Ottawa, ON K1H 8L6, Canada

⁴Clinical Epidemiology Program, Ottawa Hospital Research Institute, Ottawa, ON K1H 8L6, Canada

⁵These authors contributed equally

⁶Lead contact

*Correspondence: smei@ohri.ca

<https://doi.org/10.1016/j.isci.2022.104188>



infection. We primed MSCs with poly(I:C) (pIC), a TLR3 agonist that mimics dsRNA viral stimuli, and provided the first evidence showing an improved molecular and functional profile of primed MSCs in the context of SARS-CoV-2, leading to recalibration of the dysregulated immune response in a virus-induced inflammatory environment. In addition, pIC-MSCs showed greater inhibition of SARS-CoV-2 pseudovirus entry to human pulmonary epithelial cells *in vitro*. Compared with unprimed MSCs, pIC-MSCs further enhanced phenotypic and functional impacts on myeloid-derived populations, particularly on granulocytes and monocytes, toward less inflammatory phenotypes. These observations demonstrate that MSCs can be induced to upregulate antiviral protein expression and enhance the ability to modulate host immune responses, including direct evidence for the effects of MSCs on immune cells in the context of SARS-CoV-2, utilizing a unique *ex vivo* MSC co-culture system with whole blood from severe COVID-19 patients. Our data offer critical insights into the actions of primed MSCs in viral infections that could be leveraged for further clinical investigations.

RESULTS

Poly(I:C) stimulus enhances immunomodulatory, antiviral, and transcriptomic profile of MSCs

To study the underlying molecular changes in MSCs primed with viral mimic poly(I:C) (pIC-MSCs), we first analyzed the global transcriptome via next-generation RNA sequencing (RNAseq) at 6 h after priming. A total of 989 genes were identified to be differentially expressed, among three different donors of MSCs that had been primed with poly(I:C). Results revealed 794 upregulated and 195 downregulated genes that were modulated in pIC-MSCs compared with nonprimed cells (Ctrl-MSCs) based on Log₂ fold change cut-off criteria, < -1 indicating downregulation and >1 upregulation, with significance indicated by an adjusted p value < 0.05 (Figure 1A). Ingenuity Pathway Analysis (IPA) and Gene Ontology (GO) were conducted to gain insight into potential biological functions of the transcriptome changes. Significant enrichment (adjusted p value < 0.05) of GO terms related to defense response to the virus and interferon signaling were seen in the upregulated gene set (Figure 1B). The IPA analysis predicted a strong regulation of several canonical pathways, upstream regulators (key transcriptional regulators), and biological functions related to antiviral response (p < 0.05, Figure 1C). Negative Z score (predicts inhibition) was seen for terms such as replication of coronavirus and viral life cycle, whereas positive Z score (predicts activation) was seen for terms such as interferon signaling and maturation of blood cells. Using IPA terms to filter the dataset, we confirmed that genes induced by a pIC priming approach are primarily associated with activation of immune (411 genes) and antiviral (75 genes) responses (shown as unsupervised cluster heatmap, Figure 1D). Indeed, the most significantly upregulated genes (Top 25) included several antiviral proteins and interferon-stimulated cytokines (ISG). The protein-protein interaction analysis of these 25 upregulated protein-coding genes in pIC-MSCs suggested a relevant protein interaction (strong computational prediction) among these genes (Figure 1E). Furthermore, with UniProt Knowledgebase (UniProt Consortium, 2021), which consists of all known protein sequence data linked to functional information about that protein, we found that compared with nonprimed MSCs, pIC priming specifically increased expression of gene coding for secreted antiviral factors (Figure 1F). These data were consistent among three different MSC donors. Altogether, our data revealed dynamic transcriptome changes induced by pIC in MSCs, specifically on genes and proteins responsible for enhancing antiviral response and immunomodulatory functions.

pIC-primed MSCs show enhanced inhibition of SARS-Cov-2 pseudoviruses viral entry in vitro

To validate antiviral and immune response pathways identified in the aforementioned RNAseq analysis, proteins coded by these related genes were measured in the supernatant or cell lysate from pIC-MSCs and Ctrl-MSCs at 24 h after priming. Cytokines, including CCL2, CXCL10, CXCL11, CXCL8, and interleukin-6 (IL-6), showed significantly increased levels in conditioned media from pIC-MSCs (versus Ctrl-MSCs, Figure 2A). Western blot analysis of antiviral proteins confirmed the elevation of IFIT1 (interferon-induced protein with tetratricopeptide repeats 1), IFITM3 (interferon-induced transmembrane protein 3), Mx1 (MX dynamin-like GTPase 1), and OAS1 (2'-5'-oligoadenylate synthetase 1), but not TRIM-5α (tripartite motif-containing protein 5) or RNase L (ribonuclease L) antiviral proteins in pIC-MSCs (Figure 2B, see summarized data in Figure S1). The secretion of IFITM3, a virus host restriction factor that has been described to be released by extracellular vesicles and inhibits infections in dengue (Zhu et al., 2015) and zika (Zou et al., 2021) viral models, was increased by pIC-MSCs compared with Ctrl-MSCs (Figure 2C).

Next, to examine the potential antiviral effect of MSCs in coronavirus, SARS-CoV-2 pseudovirus tagged with a fluorescent reporter was used to evaluate viral entry in human alveolar epithelial cells (HAEPi). MSCs have been reported to not be permissive to coronavirus infection due to their lack of ACE 2

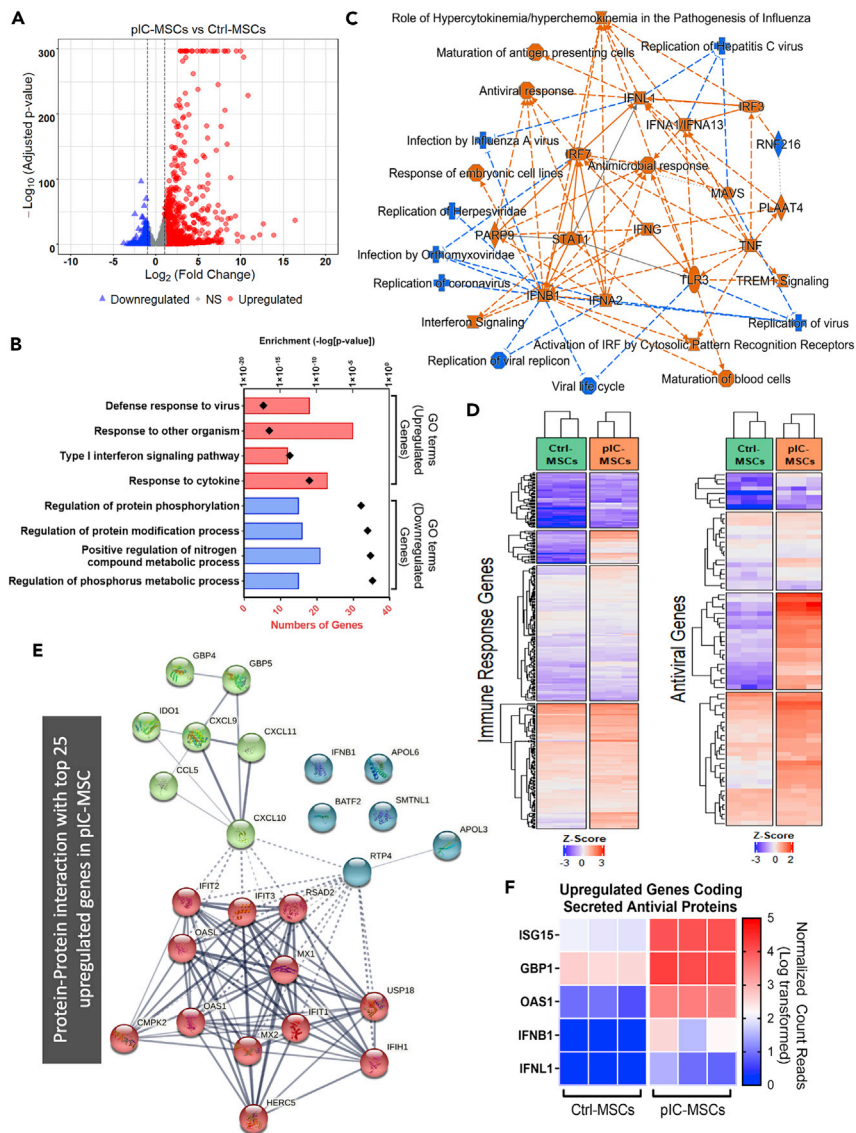


Figure 1. pIC priming enhances antiviral and immunomodulatory transcriptomic profile of MSCs

(A) Volcano plot shows differentially expressed genes (log₂ fold change >1 or <-1 and adjusted p value <0.05) with 794 genes upregulated (red) and 195 downregulated (blue); NS: nonsignificant change (gray). Each dot represents one gene.

(B) Ingenuity Pathway Analysis of the differentially expressed genes dataset showed the most significant canonical pathways, molecules, diseases, and functions. Blue icon: negative Z score (predicts inhibition); orange icons: positive Z score (predict activation).

(C) Relevant Gene Ontology terms for the top 50 upregulated (red) and downregulated (blue) genes in pIC-MSCs compared with unprimed MSCs.

(D) Heatmaps of unsupervised clustering show gene expression (normalized counts) of Ctrl-MSCs and pIC-MSCs, illustrating the variation of genes (each row) annotated for immune or antiviral response. Each column represents MSCs derived from one bone marrow donor, with a total of three donors.

(E) Protein-protein interaction network shows top 25 upregulated protein-coding genes in pIC-MSCs (cluster [k-means] numbers estimated to be 3). The thickness of the network edge line indicates the strength of publicly available data that support the specific interaction, with the thicker line indicating stronger evidence support.

(F) Heatmap showing upregulated genes in pIC-MSCs coded for secreted antiviral proteins. For RNA-seq, n = 3 biological replicates.

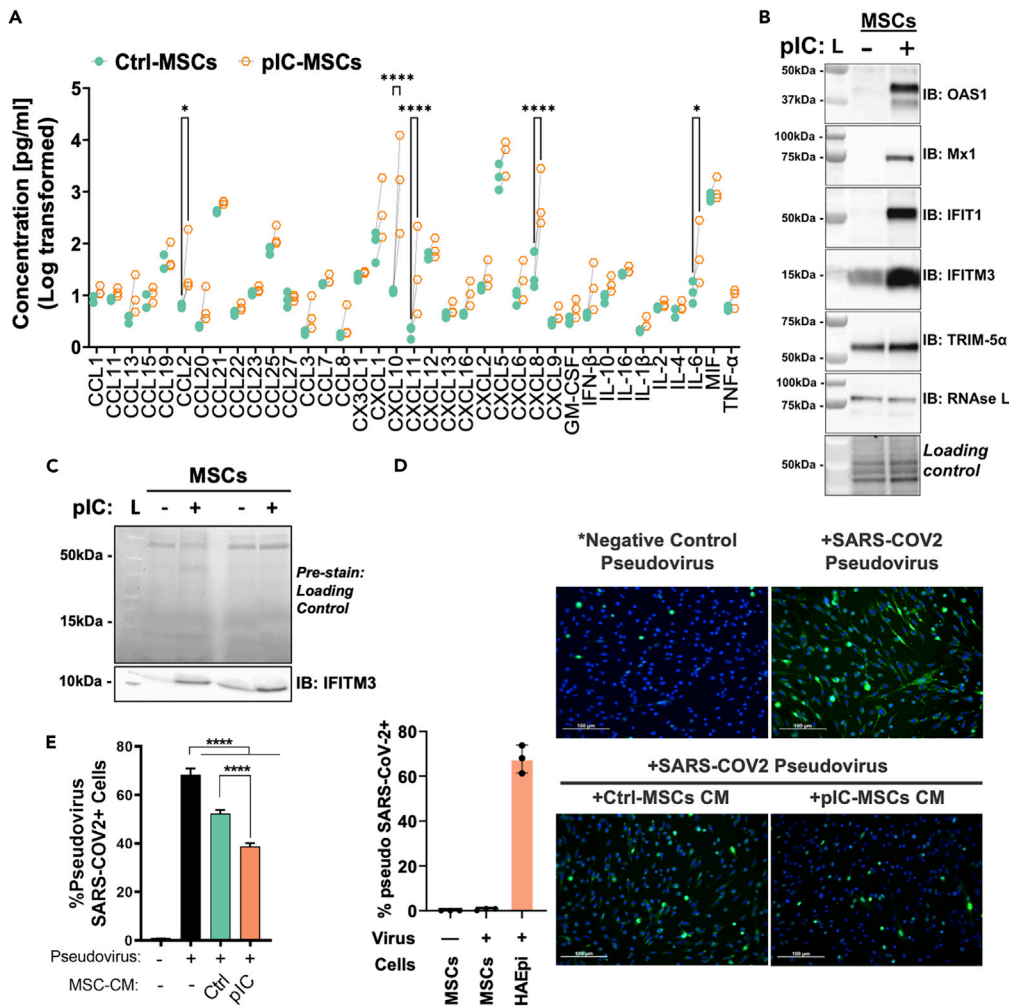


Figure 2. pIC priming enhances antiviral and immunomodulatory profile of MSCs

(A) Cytokines were measured using MSC supernatant collected after 24 h of pIC stimulation. Secretome profile showing 37 soluble factors measured in the supernatant with log-transformed data shown. Each dot represents one MSC donor, with a total of three donors included.

(B) Representative image of western blot analysis showing increased intracellular antiviral proteins in MSC lysate after 24 h of pIC priming (compared with non-pIC primed). Images obtained from chemiluminescent and colorimetric channel were merged to show molecular weight ladder position (left lane). Total proteins (run on stain-free gel) shown on bottom panel were used as loading control.

(C) Western blot analysis showing expression of secreted antiviral protein IFITM3 in MSC supernatant from two independent experiments. Images obtained from chemiluminescent and colorimetric channel were merged to show molecular weight ladder position (left lane). Total proteins (run on stain-free gel) shown on bottom panel were used as loading control.

(D) Fluorescently tagged SARS-CoV-2 pseudovirus was incubated with MSCs or human alveoli epithelial cells (HAEPi), which showed MSCs were not permissive to pseudovirus entry.

(E) Fluorescently tagged SARS-CoV-2 pseudovirus was incubated with human alveoli epithelial cells with or without MSC-conditioned media, which showed pIC-MSCs had greater effects in blocking pseudovirus entry into epithelial cells. Event was quantified by flow cytometry, and images were taken with fluorescent microscope (scale bars, 100 μ m). Summary data of the protein expression is in Figure S1. For all experiments, n = 4–6 of independent experiments with the data shown as mean \pm SEM *p < 0.05, **p < 0.01, ***p < 0.005, ****p < 0.001. For western blot images, L = molecular weight ladder and IB = immunoblotting.

(ACE2) expression (Khatiri and Saif, 2013). We exposed MSCs to the SARS-CoV-2 pseudovirus and confirmed a minimal level of pseudovirus entry could be detected in MSCs (Figure 2D). In HAEPi, SARS-CoV-2 pseudovirus exhibited efficient viral entry, with fluorescence detected in $68.3 \pm 5.2\%$ of cells. In

contrast, HAEpi cells incubated with conditioned media from Ctrl-MSCs had significantly reduced viral entry with $52.3 \pm 3.7\%$ of HAEpi SARS-CoV-2 pseudovirus positive, whereas conditioned media of pIC-MSC further augmented the ability to suppress viral entry, showing only $38.8 \pm 3.3\%$ of HAEpi cells positive for fluorescent signals (Figure 2E). Our results demonstrate that antiviral effects of MSCs can be further improved with dsRNA pIC priming.

pIC-primed MSCs more effectively modulate granulocytes and monocytes toward less inflammatory phenotypes

To confirm that pIC priming enhances the immunomodulatory effect of MSCs, we employed an *ex vivo* acute inflammation system (lipopolysaccharide [LPS]-stimulated whole blood from healthy donors incubated with or without MSC co-culture), followed by mass cytometry (CyTOF) analysis to deep profile the immune cell populations. A t-distributed stochastic neighbor embedding (tSNE) analysis was first conducted on the pan-leukocyte population identified from CyTOF, followed by self-organizing maps (FlowSOM), which showed that granulocytes formed the large metaclusters in a minimum spanning tree (MST), color mapped with CD66b expression to identify neutrophil clusters (Figure S2). Stimulation of whole blood with LPS upregulated CD14 and CD64 expression in CD66b + neutrophils (indicative of inflammatory phenotype), whereas both MSCs and pIC-MSCs suppressed this response (Figures 3A and S2). Other granulocyte-associated markers, including CD33, CD13, CD15, and HLA-DR, were also analyzed and showed no significant changes with or without MSC (Ctrl- or pIC-) treatments after LPS stimulation. A subsequent t-SNE and FlowSOM analysis of CD66b–mononuclear cells identified 10 metaclusters of immune cell subpopulations (Figure 3B), with monocytes (CD14⁺) as metacluster 1, 2, 4, 5, 6, and 7, of which expression of M1 (CD64) and M2 (CD206) polarization markers were extracted and presented as pie charts within each node (Figure 3C). Notably, we observed shifts in nodes of monocytic regions (in dotted circles) of MSTs among LPS-stimulated whole blood with or without Ctrl-MSC or pIC-MSC co-culturing (Figure 3C). In particular, pIC-MSCs significantly increased CD206 and decreased CD64 expression on monocytes, implying a further shift toward M2 polarization (Figure 3D). We next sought to determine whether this shift was associated with functional improvement in phagocytic capacity. Co-culture with pIC-MSCs more significantly improved phagocytosis ability of CD14⁺ monocytes ($p < 0.0001$ between Ctrl-MSC versus pIC-MSC, Figure 3E). We next examined changes in CD4⁺ and CD8⁺ T cell populations after MSC co-culture. Both Ctrl- or pIC-MSCs did not change the size of the CD4⁺ or CD8⁺ populations, nor the expression of activation marker HLA-DR (Figure 4A). Furthermore, in MSC and PBMC co-culture experiments, we found priming of MSCs by pIC did not impair their ability to suppress T cell proliferation or activation, compared with Ctrl-MSC (Figures 4B and 4C). Taken together, these data show that pIC priming enhanced the ability of MSCs to modulate monocytes and neutrophils toward less inflammatory phenotypes, as well as improve their phagocytic capacities under an *ex vivo* model of acute inflammation.

pIC-MSCs better modulate severe COVID-19 patient immune Cell responses in an *ex vivo* model

To evaluate whether MSCs modulate host cell responses in the context of immune dysfunction in COVID-19, we utilized an *ex vivo* co-culture system using Ctrl- or pIC-MSCs with whole blood collected from critically ill COVID-19 patients (see Table S1 for patient characteristics), followed by CyTOF analysis. The tSNE algorithm was conducted on CD45⁺ leukocytes, followed by PhenoGraph algorithm for cluster generation (Figures 5A, S3A and S3B). Phenotypic changes were identified by CyTOF to segregate major leukocyte lineages in whole blood via expression of 23 markers. On the t-SNE map, neutrophil populations formed the largest clusters (cluster 1, 2, 3, 4, 5, and 7) (Figure 5A). Using density analysis, we identified that cluster 1, 2, 3, 4, and 5 were neutrophils uniquely present in COVID-19 patients (Figure 5B), whereas neutrophils from healthy donors were in cluster 7 (Figure S3A). Furthermore, distinct phenotypic shifts in neutrophil populations in COVID-19 immune responses were observed after co-culturing with pIC-MSCs (Figure 5B). We then extracted the median intensities of neutrophil-relevant markers and generated a dot plot (Figure 5C). A side-by-side comparison of neutrophil-related marker expression in these clusters confirmed the presence of neutrophils at various levels of immaturity, with reduced expressions of CD66b and CD16 in COVID-19 patients (Figure 5C). Furthermore, we identified inflammatory neutrophil populations (CD66b + cells; clusters 4 and 5) in COVID-19 patients that exhibited high expression of CD64, a biomarker correlated with sepsis, infectious diseases, and tissue damage (Hoffmann, 2009). In contrast, pIC-MSCs increased nonactivated neutrophils (cluster 1) and reduced inflammatory neutrophil populations with high CD64 expression (cluster 4, 5) (Figure 5D). Total monocyte numbers in whole blood (cluster 6) were not affected in the presence of MSCs (Figure 5D). However, while exerting no effects on CD86 and

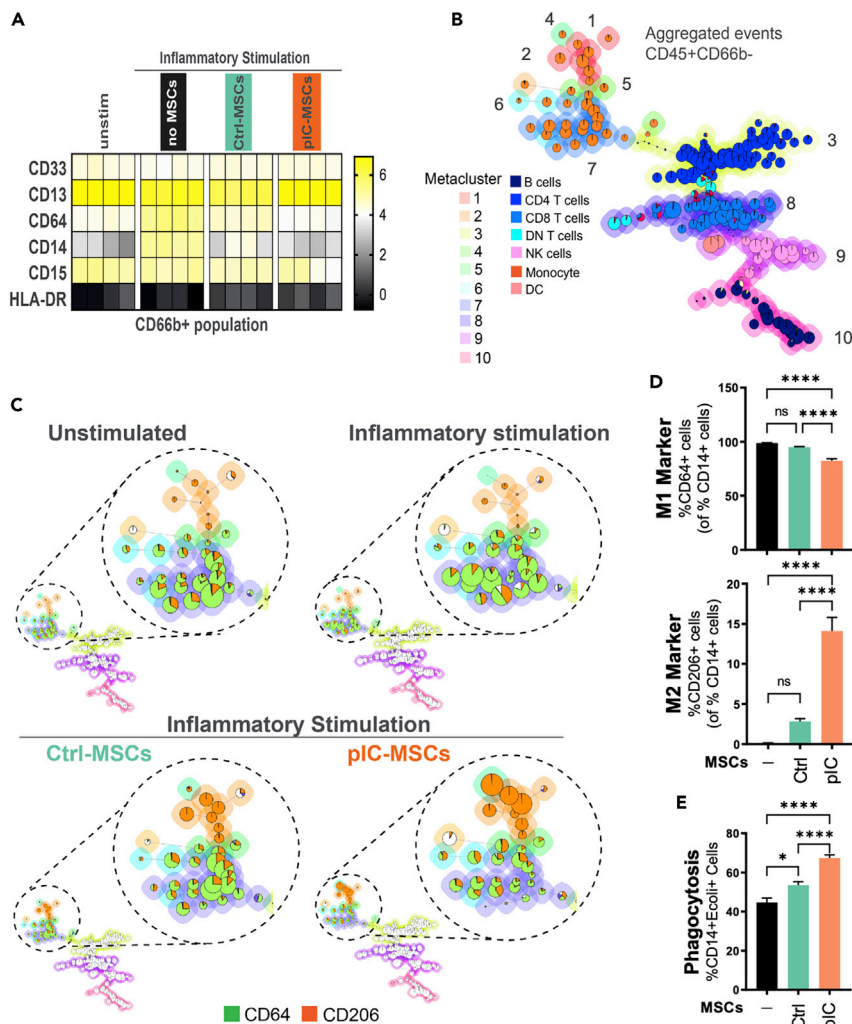


Figure 3. Enhanced ability of pIC-primed MSCs to modulate innate immune cell responses *ex vivo*

(A) Heatmap represents changes of phenotypic markers on CD66b+ cells with or without MSC co-culture upon inflammatory (LPS) stimulation.

(B) Cell subsets (10 clusters) of CD45+/CD66b- mononuclear cell population were identified by FlowSOM algorithm, with total aggregated events (100,000 single cells) shown.

(C) MST plots of unstimulated and stimulated whole blood, with or without MSCs (Ctrl-MSCs, pIC-MSCs), were shown, with details of monocyte population enlarged in dash circle. Expression of CD64 and CD206 were extracted and overlaid on MST shown as pie chart to visualize the shifts in monocyte phenotype with LPS stimulation under different co-culturing conditions.

(D) Quantification of CD64 (M1 marker) and CD206 (M2 marker) expressions of monocytes identified in (C).

(E) Phagocytic capacity of CD14+ monocytes measured with pHrodo bioparticles, showing increased phagocytosis after poly(I:C)-MSC co-culture. For all experiments, n = 4 of independent experiments with data shown as bar graphs as mean ± SEM (panel D, E). ns = nonsignificant; *p < 0.05, **p < 0.01, ***p < 0.005, ****p < 0.001. See also Figure S3.

CD64 expression, Ctrl-MSCs, and to a larger extent, pIC-MSCs, did shift the monocyte population toward a more M2 phenotype (higher CD206 and HLA-DR) (Figure 5E), consistent with our observations from LPS-stimulated healthy whole blood (Figure 3C).

Having established that pIC-MSCs exhibited enhanced modulatory effects on neutrophils and monocytes, we investigated how these phenotypic changes could translate to biological functions. After pIC-MSC co-culture, total leukocytes showed a trend in reduction of apoptosis in blood from severe COVID-19 patients (p = 0.55 for COVID-19 versus COVID-19/Ctrl-MSC, p = 0.093 for COVID-19 versus COVID-19/pIC-MSC) (Figure 5F). Furthermore, phagocytic capacity of CD66b+ neutrophils and CD14+ monocytes were

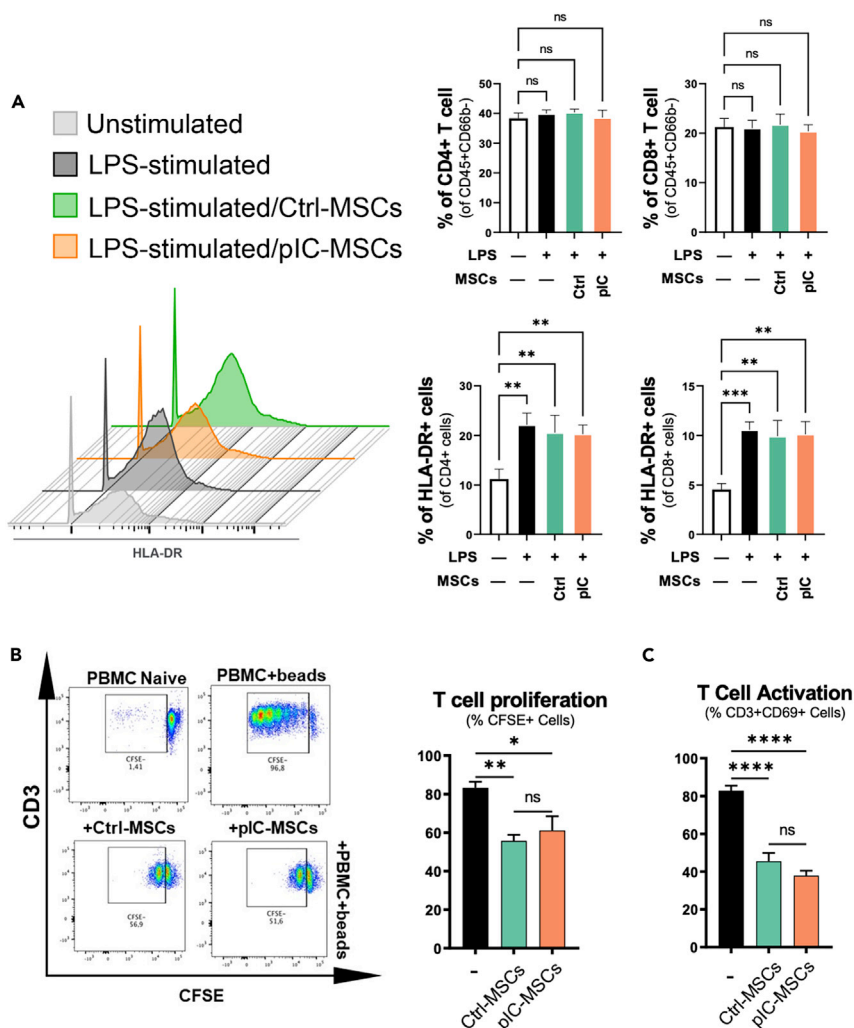


Figure 4. piC priming did not affect MSC's ability to modulate T cells

(A) Qualification of CD4⁺ and CD8⁺ T cell showed no effects on cell population by LPS stimulation with Ctrl- or piC-MSC co-culturing. Expression of HLA-DR, activation marker, on CD4⁺ and CD8⁺ T cell of CyTOF data in Figure 3A was also quantified, which showed no impact on T cell activation by MSCs (either by MSCs with or without piC-priming) co-culturing.

(B) Effect of inhibition on T cell (CFSE stained) proliferation by MSCs (Ctrl versus piC-treated). MSCs were co-cultured with the PBMCs activated with Dynabeads Human T-Activator CD3/CD28 for 5 days. On day 5, cells were stained with CD3 followed by measurement of proliferation of T cell (CD3+CFSE+) by flow cytometry (showing representative dot plots). Flow cytometric analysis showed comparable extent of inhibition on T cell proliferation by either Ctrl- or piC-MSCs, with % T cell proliferation plotted as bar graph.

(C) Effect on T cell activation by MSCs (by Ctrl-MSCs vs. piC-MSCs). MSC were co-cultured with the activated PBMCs for 2 days, followed by measurement of CD3 and CD69 to detect T cell activation status by flow cytometry. For all experiments, n = 4–6 of independent experiments with the data shown as bar graph as mean ± SEM *p < 0.05, **p < 0.01, ***p < 0.005, ****p < 0.001.

improved by Ctrl-MSC, and more so by piC-MSC co-culture (versus non-MSC treated, p < 0.01 for monocytes and p < 0.005 for neutrophils, Figure 5G).

Altogether, we found that piC-MSCs shifted neutrophil and monocyte populations in whole blood from COVID-19 patients toward a more modulatory phenotype, with enhanced phagocytic effector function. The data corroborate our findings seen in the acute inflammatory model with healthy donor whole blood stimulated by LPS, while further demonstrating that piC priming renders an enhanced immunomodulatory activity of MSCs in pathogenic viral infections.

DISCUSSION

Our study uncovers upregulation of antiviral and immunomodulatory pathways in MSCs using an *in vitro* priming strategy, leading to an improved ability for MSCs to modulate the immune landscape in acute inflammation and in COVID-19. It has been suggested that the innate potential of MSCs can be influenced by diverse extrinsic factors such as oxygen concentration and the presence/absence of various cytokines (Noronha et al., 2019). Herein, we first demonstrated that an altered transcriptome and cytokine profile toward an antiviral and improved immunomodulatory phenotype can be acquired when MSCs are primed with pIC, a viral stimuli mimic. Second, of particular importance, the present study is the first to explore how pIC-MSCs regulate antiviral protein expression while exhibiting augmented ability to modulate host innate immune responses. Third, by using an innovative *ex vivo* co-culture model with COVID-19 patient blood combined with a deep immune profile approach, we demonstrate that antiviral and immunomodulatory functions of MSC features are augmented by pIC priming on global immune cells and therefore lead to better modulation of immune responses, resulting in less inflammatory neutrophils and more M2 monocytes. Results presented here advance our understanding on how MSCs contribute their beneficial effects at the cellular and molecular level during viral infection, with important implications that may guide the design of a next-generation MSC therapy in critically ill patients with SARS-CoV-2 infection or different underlying viral etiologies.

Studies have shown that stimulation of specific TLRs affects the immune modulating responses of MSCs (Waterman et al., 2010). For example, TLR3 stimulation of human MSCs establishes their immunosuppressive effects, whereas TLR4 activation elicits proinflammatory effects (Waterman et al., 2010). The pIC-activated MSCs were also shown to be more effective in reducing sepsis-induced inflammation and organ dysfunction while improving overall survival in a mouse model of polymicrobial sepsis via upregulated miRNA-143 (Zhao et al., 2014). Pierce et al. confirmed that priming MSCs with pIC enhances expression of proteins related to host defense and innate immunity in extracellular vesicles (Pierce and Kurata, 2021). In the current study, we further demonstrate that the empowerment of MSCs by pIC priming could be a valid therapeutic approach to improve the immunomodulatory and antiviral effectiveness of MSCs to treat COVID-19. It is worth mentioning that pIC-primed MSCs exhibit an enhanced antiviral and modulated secretome profile, which ultimately stimulates greater host defense, contributing to the blocking of SARS-CoV-2 virus entry to epithelial cells.

Unlike more lineage committed cells, MSCs are known to have an inherent ability to resist viral infection with endogenous expression of interferon-stimulated cytokines, including OAS1, Mx1, and the IFITM family (Prelli Bozzo et al., 2021), targeting different stages of viral cycle (Wu et al., 2018). Herein, we highlight the upregulation of those proteins in pIC-MSC. The OAS1 protein can bind double-stranded RNA and subsequently activate the latent RNase L that, when activated, can cleave single-stranded RNAs (Rebouillat and Hovanessian, 1999). Zhou et al. provided evidence that increased OAS1 levels in humans is strongly associated with reduced risks of very severe COVID-19 hospitalization and susceptibility (Zhou et al., 2021). The Mx proteins belong to the dynamin family and have been shown to display activity against several viruses (Hefti et al., 1999; Schwemmler et al., 1995). As for the IFITM family, it has been reported these proteins can block cytosolic entry of SARS-CoV-1 and SARS-CoV-2 as well as MERS-CoV (Wrensch et al., 2014; Shi et al., 2021). Kirchhoff and colleagues recently demonstrated that exogenous overexpression of IFITM proteins in HEK293T cells prevents spike-protein-mediated fusion and SARS-CoV-2 entry.

Some preclinical studies have indicated beneficial effects of MSCs in different viral infections. A study by Qian and colleagues reported antiviral activity of MSCs against hepatitis C virus, mainly conferred by non-coding miRNAs (Qian et al., 2016). In our study, we further demonstrate that by priming MSCs with viral stimuli, pIC-MSCs can exert superior effect in blocking viral entry. Altogether, pIC-MSCs show an augmented antiviral phenotype that could contribute to more efficient inhibition of SARS-CoV-2 infection in COVID-19. In addition, the current study provides the first evidence that, coupled with upregulated antiviral pathways, pIC priming renders MSCs with improved modulatory abilities on host immune cellular responses that can be beneficial in the context of severe SARS-CoV-2 infections, likely due to elevated secretion of cytokines such as CCL2(MCP1), CXCL10(IP-10), CXCL11(I-TAC), IL-6, and CXCL8 (IL-8). These cytokines are pleiotropic cytokines in an infectious setting. There is direct evidence supporting the importance of IL-6 during viral infections, shown experimentally using IL-6-deficient mice (Lauder et al., 2013; Yang et al., 2016). IL-6 has been shown to be essential for survival of mice infected with an influenza virus by promoting optimal regulation of the T cell response, inflammatory resolution, tissue remodeling promoting lung repair, migration, and phagocytic activities of macrophages, preventing viral-induced

apoptosis in lung epithelial cells, and regulation of immunoglobulin G (IgG) isotype switching (Lauder et al., 2013; Yang et al., 2016). Trifilo et al. further demonstrated that CXCL10 expression played a pivotal role in defense following coronavirus infection of the CNS by recruitment and activation of natural killer (NK) cells that reduced viral replication (Trifilo et al., 2004). Furthermore, CCL2 is important in coordinating the immune response following microbial infection by regulating T cell polarization as well as leukocyte migration and accumulation within infected tissues (Held et al., 2004).

In our *ex vivo* model, pIC-MSCs more effectively modulate dysfunctional neutrophils toward a less inflammatory phenotype with higher phagocytic activities, while polarizing monocytes toward an M2 phenotype, which plays an important role in the resolution phase of inflammation and the repair of damaged tissues. A previous report documented a myeloid-driven immunopathology in COVID-19, in which hyperactivated neutrophils and an ineffective adaptive immune system act as mediators of the cytokine storm that worsens disease severity (Vanderbeke et al., 2021). Patients with severe COVID-19 show dysfunction in myeloid cells, with a particularly large population of immature and dysfunctional neutrophils and monocytes with an inflammation-promoting phenotype (lack of HLA-DR) (Schulte-Schrepping et al., 2020). Hyperactivated neutrophils not only play an important role in systemic COVID-19 disease manifestations but also contribute to severe COVID-19-associated pneumonia and tissue damage (van de Veerdonk et al., 2020; Barnes et al., 2020). Consistent with the existing literature, we observed that COVID-19 patients display a high level of immature neutrophils and inflammatory monocytes.

The cellular signature in severe COVID-19 patients feature a surge of HLA-DR^{low} classical monocytes, reminiscent of an immune paralysis phenotype seen in severe ARDS and sepsis. HLA-DR^{low} classical monocytes, which exhibit increased capacity in cytokine production, are a key determinant of the severity of COVID-19. These dysregulated monocytes may contribute to an insufficient antiviral immune response or may arise as a by-product of a hyperinflammatory environment (Chevrier et al., 2021). We find that MSCs primed with viral mimic pIC were enhanced in their ability to suppress neutrophil activation and skew the monocyte phenotype toward M2 phenotype (increase of CD206 and HLA-DR expression). Importantly, Trombetta et al. reported that, in samples from ICU-discharged patients, M2-like monocyte subsets were increased and contributed to an acquired myeloid cell immune-regulatory phenotype that aided in patient recovery from severe SARS-CoV-2 infection (Trombetta et al., 2021). Their data corroborate our findings that the use of a therapeutic agent, such as pIC-primed MSCs, with a capacity to induce innate immune system regulatory shift could represent a viable strategy to combat severe COVID-19 (Trombetta et al., 2021). In addition to phenotypic changes, monocytes co-cultured with pIC-MSC exhibited greater functional ability to phagocytose, which could ultimately lead to better pathogen clearance.

In summary, here we present important evidence that pIC-MSCs possess improved antiviral and immunomodulatory functions. This study highlights the immense potential of pIC-MSCs to be explored as a next-generation cell therapy for infectious diseases. Our results illustrate the ability of pIC-MSCs to reshape the immune cell landscape in severe COVID-19 directly in a disease-relevant human cellular context.

Limitations of the study

In the current study, we utilized bone-marrow-derived MSCs to investigate how pIC preconditioning affects the antiviral and immunomodulation functions of MSCs. Differences in molecular profiles have been reported among MSCs derived from various tissue sources. Here, we utilized a pseudovirus-based *in vitro* model to explore the inhibitory effect of MSCs on SARS-CoV-2 viral entry into the epithelial cells. To date, there are still limited animal models available for studying SARS-CoV-2 infection and most require the ability to access a biosafety level-3 facility. Future studies may be needed to further explore actions of MSCs or pIC-MSCs in other pathogenic aspects of virus cycle, including transmission and replication.

STAR★METHODS

Detailed methods are provided in the online version of this paper and include the following:

- KEY RESOURCES TABLE
- RESOURCE AVAILABILITY
 - Lead contact
 - Materials availability
 - Data and code availability

- **EXPERIMENTAL MODEL AND SUBJECT DETAILS**
 - Healthy volunteer and COVID-19 Cohort
 - Bone marrow aspirates and MSC culture
- **METHOD DETAILS**
 - Library preparation and sequencing
 - RNAseq data analysis
 - Conditioned media and secretome profile
 - Immunomodulatory assays to assess MSC functions
 - Mass cytometry-based immune cell profiling (CyTOF)
 - Antibodies used for mass cytometry
 - Mass cytometry data analyses
 - Pseudovirus assay
 - Immunoblot analysis
 - Immunoblot analysis of secreted proteins
- **QUANTIFICATION AND STATISTICAL ANALYSIS**

SUPPLEMENTAL INFORMATION

Supplemental information can be found online at <https://doi.org/10.1016/j.isci.2022.104188>.

ACKNOWLEDGMENTS

The authors gratefully acknowledge the support of Drs. Gareth Palidwor and Christopher Porter of the Bioinformatics Core Facility of Ottawa Hospital Research Institute for technical support on RNAseq data analysis; Dr. Damian Carragher (mass cytometry proteomic core) for providing help in CyTOF data analysis; Rebecca Porteous for supporting participant recruitment. The work was supported by ThistleDown Foundation, Emergent Ventures (Fast Grant, S.H.J.M.), The Ottawa Hospital Foundation COVID-19 Emergency Response Fund (S.H.J.M.), and Ontario Institute of Regenerative Medicine—Disease Team Grant (S.H.J.M. & L.M.).

AUTHOR CONTRIBUTIONS

L.S.M. and Y.T: Conceptualization, Data curation, Methodology, Investigation, Visualization, Formal analysis, and Writing—original draft; Y.W., J.W., and A.M: Investigation, Methodology, and Validation; M.S. and M.F: Resources; J.V: Software and Data curation; I.W: Resource—Participants' Recruitment; L.M. and S.E: Clinical Supervision, and Writing—Review & Editing; D.J.S: Supervision and Writing—Review & Editing; S.H.J.M: Conceptualization, Funding acquisition, Project administration, Supervision, Writing—Review & Editing.

DECLARATION OF INTERESTS

The funding institution had no role in the conception; design or conduct of the study; data collection or analysis; interpretation or presentation of the data; or preparation, review, or approval of the manuscript. We also like to declare the following conflicts of interest: D.J.S. is co-founder and holds equity in Northern Therapeutics Inc., and S.H.J.M. is a part-time employee of Northern Therapeutics Inc. for work outside of this study. However, these conflicts are not relevant for any of the work included in submission. The remaining authors have no disclosures.

Received: December 27, 2021

Revised: February 25, 2022

Accepted: March 30, 2022

Published: May 20, 2022

REFERENCES

Barnes, B.J., Adrover, J.M., Baxter-Stoltzfus, A., Borczuk, A., Cools-Lartigue, J., Crawford, J.M., Dassler-Plenker, J., Guerci, P., Huynh, C., Knight, J.S., et al. (2020). Targeting potential drivers of COVID-19: neutrophil extracellular traps. *J. Exp. Med.* 217, e20200652.

Bellingan, G., Jacono, F., Bannard-Smith, J., Brealey, D., Meyer, N., Thickett, D., Young, D., Bentley, A., Mcverry, B.J., Wunderink, R.G., et al. (2022). Safety and efficacy of multipotent adult progenitor cells in acute respiratory distress syndrome (MUST-ARDS): a multicentre,

randomised, double-blind, placebo-controlled phase 1/2 trial. *Intensive Care Med.* 48, 36–44.

Bruzzesi, E., Ranzenigo, M., Castagna, A., and Spagnuolo, V. (2021). Neutralizing monoclonal antibodies for the treatment and prophylaxis of

- SARS-CoV-2 infection. *New Microbiol.* 44, 135–144.
- Chen, H., Lau, M.C., Wong, M.T., Newell, E.W., Poidinger, M., and Chen, J. (2016). Cytofit: a bioconductor package for an integrated mass cytometry data analysis pipeline. *PLoS Comput. Biol.* 12, e1005112.
- Chevrier, S., Zurbuchen, Y., Cervia, C., Adamo, S., Raeber, M.E., De Souza, N., Sivapatham, S., Jacobs, A., Bachli, E., Rudiger, A., et al. (2021). A distinct innate immune signature marks progression from mild to severe COVID-19. *Cell Rep. Med.* 2, 100166.
- Dominici, M., Le Blanc, K., Mueller, I., Slaper-Cortenbach, I., Marini, F., Krause, D., Deans, R., Keating, A., Prockop, D., and Horwitz, E. (2006). Minimal criteria for defining multipotent mesenchymal stromal cells. The International Society for Cellular Therapy position statement. *Cytotherapy* 8, 315–317.
- Gu, Z., Eils, R., and Schlesner, M. (2016). Complex heatmaps reveal patterns and correlations in multidimensional genomic data. *Bioinformatics* 32, 2847–2849.
- Hefti, H.P., Frese, M., Landis, H., Di Paolo, C., Aguzzi, A., Haller, O., and Pavlovic, J. (1999). Human MxA protein protects mice lacking a functional alpha/beta interferon system against La crosse virus and other lethal viral infections. *J. Virol.* 73, 6984–6991.
- Held, K.S., Chen, B.P., Kuziel, W.A., Rollins, B.J., and Lane, T.E. (2004). Differential roles of CCL2 and CCR2 in host defense to coronavirus infection. *Virology* 329, 251–260.
- Hoffmann, J.J. (2009). Neutrophil CD64: a diagnostic marker for infection and sepsis. *Clin. Chem. Lab. Med.* 47, 903–916.
- Khatri, M., and Saif, Y.M. (2013). Influenza virus infects bone marrow mesenchymal stromal cells in vitro: implications for bone marrow transplantation. *Cell Transpl.* 22, 461–468.
- Kim, D., Paggi, J.M., Park, C., Bennett, C., and Salzberg, S.L. (2019). Graph-based genome alignment and genotyping with HISAT2 and HISAT-genotype. *Nat. Biotechnol.* 37, 907–915.
- Kotecha, N., Krutzik, P.O., and Irish, J.M. (2010). Web-based analysis and publication of flow cytometry experiments. *Curr. Protoc. Cytom. Chapter 10, Unit 10.17.* <https://doi.org/10.1002/0471142956.cy1017s53>.
- Lanzoni, G., Linetsky, E., Correa, D., Messinger Cayetano, S., Alvarez, R.A., Kouroupis, D., Alvarez Gil, A., Poggioli, R., Ruiz, P., Martos, A.C., et al. (2021). Umbilical cord mesenchymal stem cells for COVID-19 acute respiratory distress syndrome: a double-blind, phase 1/2a, randomized controlled trial. *Stem Cells Transl. Med.* 10, 660–673.
- Lauder, S.N., Jones, E., Smart, K., Bloom, A., Williams, A.S., Hindley, J.P., Ondondo, B., Taylor, P.R., Clement, M., Fielding, C., et al. (2013). Interleukin-6 limits influenza-induced inflammation and protects against fatal lung pathology. *Eur. J. Immunol.* 43, 2613–2625.
- Leng, Z., Zhu, R., Hou, W., Feng, Y., Yang, Y., Han, Q., Shan, G., Meng, F., Du, D., Wang, S., et al. (2020). Transplantation of ACE2. *Aging Dis.* 11, 216–228.
- Levine, J.H., Simonds, E.F., Bendall, S.C., Davis, K.L., Amir, E.-A., Tadmor, M.D., Litvin, O., Fienberg, H.G., Jager, A., Zunder, E.R., et al. (2015). Data-driven phenotypic dissection of AML reveals progenitor-like cells that correlate with prognosis. *Cell* 162, 184–197.
- Love, M.I., Huber, W., and Anders, S. (2014). Moderated estimation of fold change and dispersion for RNA-seq data with DESeq2. *Genome Biol.* 15, 550.
- Matthay, M.A., Calfee, C.S., Zhuo, H., Thompson, B.T., Wilson, J.G., Levitt, J.E., Rogers, A.J., Gotts, J.E., Wiener-Kronish, J.P., Bajwa, E.K., et al. (2019). Treatment with allogeneic mesenchymal stromal cells for moderate to severe acute respiratory distress syndrome (START study): a randomised phase 2a safety trial. *Lancet Respir. Med.* 7, 154–162.
- McIntyre, L.A., Stewart, D.J., Mei, S.H.J., Courtman, D., Watpool, I., Granton, J., Marshall, J., Dos Santos, C., Walley, K.R., Winston, B.W., et al. (2018). Cellular immunotherapy for septic shock. A phase I clinical trial. *Am. J. Respir. Crit. Care Med.* 197, 337–347.
- Metcalfe, S.M. (2020). Mesenchymal stem cells and management of COVID-19 pneumonia. *Med. Drug Discov.* 5, 100019.
- Noronha, N.C., Mizukami, A., Calíari-Oliveira, C., Cominal, J.G., Rocha, J.L.M., Covas, D.T., Swiech, K., and Malmegrim, K.C.R. (2019). Priming approaches to improve the efficacy of mesenchymal stromal cell-based therapies. *Stem Cell Res. Ther.* 10, 131.
- Pierce, L.M., and Kurata, W.E. (2021). Priming with toll-like receptor 3 agonist poly(I:C) enhances content of innate immune defense proteins but not MicroRNAs in human mesenchymal stem cell-derived extracellular vesicles. *Front. Cell Dev. Biol.* 9, 676356.
- Prelli Bozzo, C., Nchioua, R., Volcic, M., Koepke, L., Krüger, J., Schütz, D., Heller, S., Stürzel, C.M., Kmiec, D., Conzelmann, C., et al. (2021). IFITM proteins promote SARS-CoV-2 infection and are targets for virus inhibition in vitro. *Nat. Commun.* 12, 4584.
- Qian, X., Xu, C., Fang, S., Zhao, P., Wang, Y., Liu, H., Yuan, W., and Qi, Z. (2016). Exosomal MicroRNAs derived from umbilical mesenchymal stem cells inhibit hepatitis C virus infection. *Stem Cells Transl. Med.* 5, 1190–1203.
- Rebouillat, D., and Hovanessian, A.G. (1999). The human 2',5'-oligoadenylate synthetase family: interferon-induced proteins with unique enzymatic properties. *J. Interferon Cytokine Res.* 19, 295–308.
- Ringdén, O., Uzunel, M., Rasmusson, I., Remberger, M., Sundberg, B., Lönnies, H., Marschall, H.U., Dlugosz, A., Szakos, A., Hassan, Z., et al. (2006). Mesenchymal stem cells for treatment of therapy-resistant graft-versus-host disease. *Transplantation* 81, 1390–1397.
- Schulte-Schrepping, J., Reusch, N., Paclik, D., Baßler, K., Schlickeiser, S., Zhang, B., Krämer, B., Krammer, T., Brumhard, S., Bonaguro, L., et al. (2020). Severe COVID-19 is marked by a dysregulated myeloid cell compartment. *Cell* 182, 1419–1440.e23.
- Schwemmle, M., Weining, K.C., Richter, M.F., Schumacher, B., and Staeheli, P. (1995). Vesicular stomatitis virus transcription inhibited by purified MxA protein. *Virology* 206, 545–554.
- Shi, G., Kenney, A.D., Kudryashova, E., Zani, A., Zhang, L., Lai, K.K., Hall-Stoodley, L., Robinson, R.T., Kudryashov, D.S., Compton, A.A., and Yount, J.S. (2021). Opposing activities of IFITM proteins in SARS-CoV-2 infection. *EMBO J.* 40, e106501.
- Snel, B., Lehmann, G., Bork, P., and Huynen, M.A. (2000). STRING: a web-server to retrieve and display the repeatedly occurring neighbourhood of a gene. *Nucleic Acids Res.* 28, 3442–3444.
- Squillaro, T., Peluso, G., and Galderisi, U. (2016). Clinical trials with mesenchymal stem cells: an update. *Cell Transpl.* 25, 829–848.
- Tan, Y., Salkhordeh, M., Wang, J.P., Mcrae, A., Souza-Moreira, L., McIntyre, L., Stewart, D.J., and Mei, S.H.J. (2019). Thawed mesenchymal stem cell product shows comparable immunomodulatory potency to cultured cells in vitro and in polymicrobial septic animals. *Sci. Rep.* 9, 18078.
- Trifilo, M.J., Montalto-Morrison, C., Stiles, L.N., Hurst, K.R., Hardison, J.L., Manning, J.E., Masters, P.S., and Lane, T.E. (2004). CXCL10 chemokine ligand 10 controls viral infection in the central nervous system: evidence for a role in innate immune response through recruitment and activation of natural killer cells. *J. Virol.* 78, 585–594.
- Trombetta, A.C., Farias, G.B., Gomes, A.M.C., Godinho-Santos, A., Rosmaninho, P., Conceição, C.M., Laia, J., Santos, D.F., Almeida, A.R.M., Mota, C., et al. (2021). Severe COVID-19 recovery is associated with timely acquisition of a myeloid cell immune-regulatory phenotype. *Front. Immunol.* 12, 691725.
- UniProt Consortium. (2021). UniProt: the universal protein knowledgebase in 2021. *Nucleic Acids Res.* 49 (D1), D480–D489.
- van de Veerdonk, F.L., Looijen-Salamon, M., van den Heuvel, M., van der Mast, Q., van der Meer, C., Vos, S., van Belle, S., Vermorgen, S., van der Hoeven, J.G., Netea, M.G., and Grünberg, K. (2020). Plasma cells and endothelitis in COVID-19 lung pathology. *SSRN Electron. J.* Available at SSRN. <https://doi.org/10.2139/ssrn.3596608>.
- Van Gassen, S., Callebaut, B., van Helden, M.J., Lambrecht, B.N., Demeester, P., Dhaene, T., and Saeys, Y. (2015). FlowSOM: using self-organizing maps for visualization and interpretation of cytometry data. *Cytometry A* 87, 636–645.
- Vanderbeke, L., van Mol, P., van Herck, Y., De Smet, F., Humblet-Baron, S., Martinod, K., Antoranz, A., Arijis, I., Boeckx, B., Bosisio, F.M., et al. (2021). Monocyte-driven atypical cytokine storm and aberrant neutrophil activation as key mediators of COVID-19 disease severity. *Nat. Commun.* 12, 1–15.
- Waterman, R.S., Tomchuck, S.L., Henkle, S.L., and Betancourt, A.M. (2010). A new mesenchymal

stem cell (MSC) paradigm: polarization into a pro-inflammatory MSC1 or an immunosuppressive MSC2 phenotype. *PLoS One* 5, e10088.

Wrensch, F., Winkler, M., and Pohlmann, S. (2014). IFITM proteins inhibit entry driven by the MERS-coronavirus spike protein: evidence for cholesterol-independent mechanisms. *Viruses* 6, 3683–3698.

Wu, X., Dao Thi, V.L., Huang, Y., Billerbeck, E., Saha, D., Hoffmann, H.H., Wang, Y., Silva, L.A.V., Sarbanes, S., Sun, T., et al. (2018). Intrinsic immunity shapes viral resistance of stem cells. *Cell* 172, 423–438.e25.

Yang, R., Masters, A.R., Fortner, K.A., Champagne, D.P., Yanguas-Casás, N., Silberger, D.J., Weaver, C.T., Haynes, L., and Rincon, M.

(2016). IL-6 promotes the differentiation of a subset of naive CD8+ T cells into IL-21-producing B helper CD8+ T cells. *J. Exp. Med.* 213, 2281–2291.

Yang, X., Yu, Y., Xu, J., Shu, H., Xia, J., Liu, H., Wu, Y., Zhang, L., Yu, Z., Fang, M., et al. (2020). Clinical course and outcomes of critically ill patients with SARS-CoV-2 pneumonia in Wuhan, China: a single-centered, retrospective, observational study. *Lancet Respir. Med.* 8, 475–481.

Zhao, X., Liu, D., Gong, W., Zhao, G., Liu, L., Yang, L., and Hou, Y. (2014). The toll-like receptor 3 ligand, poly(I:C), improves immunosuppressive function and therapeutic effect of mesenchymal stem cells on sepsis via inhibiting MIR-143. *Stem Cells* 32, 521–533.

Zhou, S., Butler-Laporte, G., Nakanishi, T., Morrison, D.R., Afilalo, J., Afilalo, M., Laurent, L., Pietzner, M., Kerrison, N., Zhao, K., et al. (2021). A Neanderthal OAS1 isoform protects individuals of European ancestry against COVID-19 susceptibility and severity. *Nat. Med.* 27, 659–667.

Zhu, X., He, Z., Yuan, J., Wen, W., Huang, X., Hu, Y., Lin, C., Pan, J., Li, R., Deng, H., et al. (2015). IFITM3-containing exosome as a novel mediator for anti-viral response in dengue virus infection. *Cell Microbiol.* 17, 105–118.

Zou, X., Yuan, M., Zhang, T., Zheng, N., and Wu, Z. (2021). EVs containing host restriction factor IFITM3 inhibited ZIKV infection of fetuses in pregnant mice through trans-placenta delivery. *Mol. Ther.* 29, 176–190.

STAR★METHODS

KEY RESOURCES TABLE

REAGENT or RESOURCE	SOURCE	IDENTIFIER
Antibodies		
Anti-human CD3- BUV395	BD Biosciences	564000;RRID:AB_2744382;
Anti-human CD14-BV421	BD Biosciences	563743; RRID:AB_2744289
Anti-human CD66B-Alexa647	BD Biosciences	561645
Anti-human CD69-BV421	BD Biosciences	562884
Anti-human CD66b	Fluidigm	3152011C
Anti-human CD15 (SSEA-1)	Fluidigm	3172021C
Anti-human CD294 (CRTH2)	Fluidigm	3163003C
Anti-human CD3	Fluidigm	3154003C
Anti-human CD279 (PD-1)	Fluidigm	3155009C
Anti-human CD14	Fluidigm	3148010C
Anti-human CD16	Fluidigm	3145008C
Anti-human CD19	Fluidigm	3169011C
Anti-human CD127 (IL-7Ra)	Fluidigm	3165008C
Anti-human CD13	Fluidigm	3160014C
Anti-human CD11b (Mac-1)	Fluidigm	3209003C
Anti-human CD44	Fluidigm	3150018C
Anti-human CD45	Fluidigm	3089003C
Anti-human CD66b	Fluidigm	3152011C
Anti-human CD33	Fluidigm	3158001C
Anti-human CD64	Fluidigm	3146006C
Anti-human CD206 (MMR)	Fluidigm	3168008C
Anti-human HLA-DR	Fluidigm	3173005C
Anti-human CD161	Fluidigm	3159004C
Anti-human CD20	Fluidigm	3171012C
Anti-human CD11c	Fluidigm	3147008C
Anti-human CD86	Fluidigm	3156008C
Anti-human Nkp44	R&D System	MAB22491; RRID:AB_2149423
Anti-human CD4	Fluidigm	3174004C
Anti-human CD8a	Fluidigm	3162015C
Anti-human IFIT1	Cell Signaling	14769S; RRID:AB_2783869
Anti-human TRIM5a (D6Z8L)	Cell Signaling	14326; RRID:AB_2798451
Anti-human RNase L (D4B4J)	Cell Signaling	27281; RRID:AB_2798941
Anti-human OAS1 (D1W3A)	Cell Signaling	14498; RRID:AB_2798498
Anti-human MX1 (D3W7I)	Cell Signaling	37849; RRID:AB_2799122
Anti-human BST2 (D5V5Z)	Cell Signaling	19277; RRID:AB_2798815
Anti-human IFITM1	Cell Signaling	13126; RRID:AB_2798126
Anti-human IFITM3 (D8E8G) XP®	Cell Signaling	59212; RRID:AB_2799561
Biological samples		
Healthy Whole Blood	STEMCELL Technologies & OHRI	REB ID: 20200312-01H
Bone Marrow Aspirates	Lonza, OHRI	REB ID: 20120929-01 H
Patient Blood Samples	The Ottawa Hospital	REB ID: #20190401-01H

(Continued on next page)

Continued

REAGENT or RESOURCE	SOURCE	IDENTIFIER
Chemicals, peptides, and recombinant proteins		
Polyinosinic–polycytidylic acid potassium salt	Sigma	P9582
BD Cytofix Fixation Buffer	BD Biosciences	554655
MSC NutriStem® XF Medium (Basal Medium + Supplement)	Biological Industries	05-200-1A-KT
Alveolar Epithelial Medium-phenol red free	ScienceCell	3201-PRF
Protease Inhibitor Cocktail	Sigma-Aldrich	535140-1ML
RIPA Lysis and Extraction Buffer	Thermo-Fisher	89901
Cell Signaling Lysis buffer	Sigma-Millipore	43-040
Criterion TGX Stain Free, 4-20%	Bio-Rad	5678095
Precision Plus Protein All Blue Standards	Bio-Rad	1610373
Clarity Max Western ECL Substrate,	Bio-Rad	1705062
Low Fluorescence PVDF membrane	Bio-Rad	1704275
pHrodo Green E.coli bioparticle	ThermoFisher	P35366
Dynabeads Human T-Activator CD3/CD28	GibCo	11161D
Annexin V	BD Biosciences	560506
Propidium iodide	ThermoFisher	P1304MP
Stable-lyse V2	Smart Tube/Fisher	501351694
Stable-store V2	Smart Tube/Fisher	501351693
SARS-CoV-2 pseudovirus	Montana Molecular	C1110G
CFSE	Thermofisher	
Critical commercial assays		
QuantiTect® Reverse Transcription Kit	Qiagen	205311
Bio-Plex Pro™ Human Chemokine Panel, 40-Plex	Bio-Rad	171AK99MR2
ExoQuick-TC	SBI	EXOTC50A-1
Cell-ID 20-Plex Pd Barcoding Kit	Fluidigm	201060
Cell-IDTM Intercalator-Ir 500 μM	Fluidigm	201192B
EQ Four Element Calibration Beads	Fluidigm	201078
UltraComp eBeads™ Compensation Beads	Thermofisher	01-2222-41
MaxPar X8 labeling kit	Fluidigm	201300
Deposited data		
Human reference genome GRCh38.13	NCBI Genome Reference	https://www.ncbi.nlm.nih.gov/assembly/GCF_000001405.39/
Raw Sequencing Data	NCBI	https://dataview.ncbi.nlm.nih.gov/object/PRJNA735444?reviewer=r7n3li5lsbcsbfbrukt943d5b ; NCBI BioProject: PRJNA735444.; https://fairsharing.org/FAIRsharing.aqhv1y
Additional Raw Data	Mendeley Dataset	https://doi.org/10.17632/wkhswx3nf8.2
Experimental models: Cell lines		
Human pulmonary alveoli epithelial cells (HAEpi)	ScienCell	3200
Software and algorithms		
R software (version 3.6.3)	r-project.org	https://www.r-project.org/
RStudio (version 1.2.5033)	RStudio Server Open-Source	https://www.rstudio.com/products/rstudio/#rstudio-desktop
HISAT2	Kim, Paggi et al. 2019	https://daehwankimlab.github.io/hisat2/

(Continued on next page)

Continued

REAGENT or RESOURCE	SOURCE	IDENTIFIER
Prism 9.0	Graphpad	https://www.graphpad.com/scientific-software/prism/
FlowJo X software	FlowJo, LLC/BD Biosciences	https://www.flowjo.com/
Bio-Plex Manager	Bio-Rad	https://www.bio-rad.com/en-ca/product/bio-plex-manager-software-standard-edition?ID=5846e84e-03a7-4599-a8ae-7ba5dd2c7684
QIAGEN Ingenuity Pathway Analysis	Qiagen	https://digitalinsights.qiagen.com/products-overview/discovery-insights-portfolio/analysis-and-visualization/qiagen-ipa/
DESeq2 version 1.26	Love et al., (2014)	https://bioconductor.org/packages/release/bioc/html/DESeq2.html
g:GOST (g:Profiler)	ELIXIR infrastructure	https://biit.cs.ut.ee/gprofiler/gost
ggplot2		https://ggplot2.tidyverse.org/
Complex Heatmap	Gu et al., (2016)	http://bioconductor.org/packages/release/bioc/html/ComplexHeatmap.html
Cytofit	Chen et al., (2016)	https://github.com/JinmiaoChenLab/cytofit
cytofAsinh	Chen et al., (2016)	https://bioconductor.riken.jp/packages/3.3/bioc/html/cytofit.html
Cytobank	Kotecha et al., (2010)	https://cytobank.org/
FlowSOM	Van Gassen et al., 2015	https://support.cytobank.org/hc/en-us/articles/360018965212-Introduction-to-FlowSOM-in-Cytobank https://bioconductor.riken.jp/packages/3.3/bioc/html/cytofit.html
PhenoGraph	Levine et al., (2015)	https://bioconductob.riken.jp/packages/3.3/bioc/html/cytofcyt.html https://www.flowjo.com/exchange/#/plugin/profile?id=1
Biorender		https://biorender.com/
String-db	Snel et al., (2000)	https://string-db.org/
Other		
Bio-Plex 200	Bio-Rad	https://www.bio-rad.com/en-ca/product/bio-plex-200-systems?ID=715b85f1-6a4e-41b3-b5d9-80202d779e13
LSRFortessa cytometer	BD Bioscience	https://www.bdbiosciences.com/en-in/instruments/research-instruments/research-cell-analyzers/lrfortessa
Attune NxT acoustic focusing cytometer	ThermoFisher	https://www.thermofisher.com/ca/en/home/life-science/cell-analysis/flow-cytometry/flow-cytometers/attune-nxt-flow-cytometer.html
Helios 2 mass cytometer	Fluidigm	https://www.fluidigm.com/products/helios

RESOURCE AVAILABILITY

Lead contact

Further information and requests for resources and reagents should be directed to and will be fulfilled by the Lead Contact, Shirley Hsin-Ju Mei (smei@ohri.ca).

Materials availability

This study did not generate new unique reagents.

Data and code availability

- The RNA-seq sequence data have been deposited at the NCBI and are publicly available as of the date of publication. Accession numbers are listed in the key resources table.

- Original Raw data from [Figures 2, 3, 4, and 5](#) have been deposited at the Mendeley and are publicly available as of the date of publication. The DOI is listed in the key resources table.
- This paper does not report original code. The publicly available scripts used to generate the figures reported in this paper are described in the STAR Methods and listed in the key resources table.

Any further questions or request for additional information to reproduce this work can be directed to the Lead Contact.

EXPERIMENTAL MODEL AND SUBJECT DETAILS

Healthy volunteer and COVID-19 Cohort

This study was approved by the Research Ethics Board (REB) (Ottawa Health Science Network REB, REB ID: 20200312-01H and #20190401-01H). After providing written informed consent, 4 health donors and 4 COVID-19 patients were included in the study. Information on age, sex, and blood analysis of healthy volunteers and COVID-19 patients were listed in [Table S1](#). COVID-19 patients who tested positive for SARS-CoV-2 were recruited in intensive care unit of The Ottawa Hospital between June 2020 and February 2021.

Bone marrow aspirates and MSC culture

Bone marrow aspirates were obtained from commercial vendor (Lonza) or at The Ottawa Hospital (with informed written consent and ethical approval granted by the Ottawa Health Science Network Research Ethics Board, REB ID: 20120929-01 H). Human bone marrow-derived MSC (n = 3 different donors; 2 females and 1 male) were cultured, characterized, and cryopreserved. Briefly, the human bone marrow aspirates were diluted, counted, and plated on T-175 flasks (Corning) with complete MSC Nutristem xeno-free media (Biological Industries) with gentamicin reagent solution [Gibco]. All cells were maintained at 37 °C, 5% (v/v) CO₂. Upon >80% confluence, MSCs were harvested and cryopreserved at 2.5 × 10⁶ cells/mL in freezing media (Biological Industries) with storage in liquid nitrogen ([Tan et al., 2019](#), [McIntyre et al., 2018](#)). MSCs have been characterized to meet all the criteria (plastic adherence, differentiation potential, and cell surface antigen expression) proposed by the International Society for Cellular Therapy (ISCT) ([Dominici et al., 2006](#)) as previously described ([Tan et al., 2019](#), [McIntyre et al., 2018](#)). Cryopreserved MSCs were thawed and cultured in Nutristem complete media (Biological Industries) for 24-72 hours prior to being lifted and plated for *in vitro* or *ex vivo* assays. MSCs were maintained at 37°C in a humidified incubator containing 5% CO₂. All experiments used cells between passages 3 to 5.

For viral stimulus priming, MSC were incubated with or without 10 µg/mL of Poly(I:C) (pIC) for 6 hours for sample collection for RNAseq analysis, or 24 hours for protein expression (total cell lysate and secreted protein in the supernatant).

METHOD DETAILS

Library preparation and sequencing

MSCs (n = 3 different donors) were incubated with or without pIC for 6 hours, then cell pellets were collected and sent to Qiagen NextGeneration Service for RNA isolation and library preparation. In summary, the libraries' size distribution was validated and quality inspected on a Bioanalyzer 2100 or BioAnalyzer 4200 TapeStation (Agilent Technologies); Sequencing was performed on an Illumina NextSeq500 instrument (76 cycles) generating single-end reads; Qiagen service reported an average 38.2 million reads were obtained for each sample.

RNAseq data analysis

In summary, raw counts were compiled into FASTQ format and the reads containing adapter sequences or qualified as low-quality reads were filtered from the dataset. All samples passed the FASTQC Quality Scores (i.e., per sequence quality scores, sequence quality histograms and adapter content). Quality controlled FASTQ files were aligned to human reference genome GRCh38.p13 using HISAT2 aligner software ([Kim et al., 2019](#)) to obtain the raw counts matrix. Data was mapped and count matrix were generated by Bioinformatics Department at OHRI. The R programming language (R version 3.6.3 and RStudio version 1.2.5033) was used to perform the gene expression analysis of the reads. Differential expression analysis was performed using the default parameters of R DEseq2 package version 1.26 (results summarized in a

volcano plot) (Love et al., 2014). RNAseq heatmaps were drawn using Complex heatmap package (Gu et al., 2016) and illustrate the variation of selected genes (each row); each column represents MSC derived from 1 bone marrow donor (n = 3 donor). The g:GOST (g:Profiler) was used for Gene Ontology analysis and to identify the enriched terms of biological process. Ingenuity Pathway Analysis software (IPA; Qiagen) was used to identify canonical pathways. String-db was used to visualize the protein-protein interaction network of the up-regulated differentially expressed genes (Snel et al., 2000).

Conditioned media and secretome profile

MSCs were primed for 24 hours without or with pIC (10 µg/mL) for 24h. The supernatant was harvested and cell debris eliminated by spinning down at 5,000g 5 min at room temperature. Supernatant was collected and stored at -80 °C. Cytokines, chemokines, and growth factors contents were detected by Multiplex Immunoassay System (Bio-Rad) in the supernatant following manufacturers' recommended protocols. Assays were conducted by personnel blinded to the identities of the sample. Alternatively, after the treatment, the supernatant was removed, and the cells were washed 3 times with PBS. Fresh media was added, and the supernatant was collected 24 hours later to produce the MSC-conditioned media.

Immunomodulatory assays to assess MSC functions

For *ex vivo* assays, whole blood (sodium citrate as anticoagulant) from healthy volunteers were obtained from commercial vendor (StemCell Technologies) or from healthy volunteer and COVID-19 patient at OHRI. Whole blood was directly co-cultured with MSCs (primed with or without pIC) for 24 hours. Blood obtained from health volunteers were used to establish *ex vivo* acute inflammation system. In summary, whole blood was co-cultured with or without MSCs in the presence of lipopolysaccharide (100 ng/mL). Whole blood and MSC co-culture were conducted in ratio of 0.5 mL of whole blood to 100,000 MSCs.

After co-culture, part of whole blood was saved for CyTOF (details below), the rest of whole blood samples underwent red blood cell lysis (ThermoFisher) to obtain total white blood cells. Cells were washed with flow cytometry washing buffer (PBS supplemented with 2% fetal bovine serum). For apoptosis staining, cells were incubated with AnnexinV (BD Biosciences) and PI (ThermoFisher) for 15 minutes at room temperature followed by flow cytometry analysis (Attune NxT acoustic focusing cytometer, ThermoFisher).

For phagocytosis analysis, pHrodo *E.coli* bioparticle (ThermoFisher) was added to whole blood culture system and incubated for 15 minutes at 37°C. Cells were then washed and stained with anti-human CD14 and anti-human CD66b (BD Biosciences) for 30 minutes at 4°C. After staining, washed cells were analyzed by flow cytometry (LSRFortessa cytometer, BD Biosciences).

In addition, the inhibition of T cell proliferation assay used peripheral blood mononuclear cells (PBMCs) stained with carboxyfluorescein succinimidyl ester (CFSE) (ThermoFisher) and activated with Dynabeads Human T-Activator CD3/CD28 (Gibco). MSCs were co-cultured with the activated PBMCs for 5 days, then the proliferation of T cell was measured by flow cytometry (Attune NxT acoustic focusing cytometer, ThermoFisher). Alternatively, cells were cultivated for 2 days and CD3 and CD69 were used to detect T cell activation status by flow cytometry. Data analysis was done using FlowJo X software (FlowJo, LLC).

Mass cytometry-based immune cell profiling (CyTOF)

For CyTOF sample processing, 250 µL of human whole blood (sodium citrate) was lysed in 350 µL of stable-lyse V2 and then fixed in 1 mL of stable-store V2 (Smart Tube Inc., San Carlos, US) as described in the user's manual and stored at -80°C until further processing. Further, whole blood samples were thawed and washed, followed by barcoding using Cell-ID 20-Plex Pd Barcoding Kit (Fluidigm). Up to 4 individual samples were barcoded for 30 minutes at room temperature. Cells were then washed and pooled for surface staining. For surface staining, cells were resuspended in diluted human Fc-block (BDbioscience) for 10 minutes and incubated with antibody staining cocktails for 30 minutes at room temperature. After incubation, cells were washed with staining buffer and fixed overnight in MaxPar Fix-I buffer with iridium intercalator (Fluidigm). Immediately prior to data acquisition, samples were washed once with each of Cell Staining Buffer (Fluidigm) and Cell Acquisition Solution (Fluidigm). Samples were then resuspended at a concentration of 5×10^5 cells per mL in Cell Acquisition Solution containing EQ Four Element Calibration Beads (5:1 Ratio) (Fluidigm). The samples were acquired on a Helios Mass Cytometer equipped with a wide-bore sample injector at a rate of 300-500 events per second. After acquisition, repeat acquisitions of the

same sample were concatenated as necessary and normalized using the Fluidigm software. Normalized fcs files were gated to exclude debris, doublets, and dead cells using Cytobank software.

Antibodies used for mass cytometry

All anti-human pre-conjugated to metal isotopes were obtained from Fluidigm Corporation (San Francisco, US). All remaining antibodies were obtained from the indicated companies as purified antibodies and in-house conjugation was completed using the MaxPar X8 labeling kit (Fluidigm) following manufacturers' recommended protocols. A detailed list of all antibodies is shown in the Key Resource table.

Mass cytometry data analyses

Files were processed following Fluidigm recommendation, including randomization and normalization using EQ Beads signal. Files were then concatenated, debarcoded, and randomized according to Fluidigm's instructions using the CyTOF Software. Gating to identify and export single cells was completed in Cytobank (Kotecha et al., 2010). Clustering analysis was completed with either FlowSOM (Cytobank)(Van Gassen et al., 2015) or PhenoGraph (Levine et al., 2015) as stated as part of the R Bioconductor package Cytokit (Chen et al., 2016) and Flowjo X using the markers listed in the Key Resource Table with up to 50,000 cells per sample. The transformation method used was cytofAsinh, and the visualization method was t-SNE. The t-SNE map overlaid with PhenoGraph-defined cell populations (Figures S3B and 4B) was generated using ggplot2 package in RStudio (open-source) and FlowJo (BD Biosciences).

Pseudovirus assay

Human pulmonary alveoli epithelial cells (HAEPi) (ScienCell Research Laboratories) were thawed and expanded in Alveolar Epithelial Cell Medium (AEPiCM) (ScienCell Research Laboratories) between passage 3-8. HAEPi were passaged into a 24-well plate overnight. On the next day, MSC-conditioned media was mixed 1:1 with AEPiCM and added to HAEPi. After one day, SARS-CoV-2 pseudovirus (Montana Molecular) was added according to manufacturer's instructions. On the following day, pseudovirus entry was measured in the harvested and washed HAEPi using flow cytometry (Attune NxT acoustic focusing cytometer, ThermoFisher).

Immunoblot analysis

Cells were collected after stimulation pIC by cell scraper and addition of sample lysis buffer (Sigma-Millipore). Protein quantification was performed using Bradford reagent (Bio-Rad). Loading buffer was added to the cell lysate, and immediately heated at 95°C for 5 minutes. Samples (10-15 µg of protein/lane) were resolved by electrophoresis on pre-cast SDS-PAGE(Bio-Rad). After electrophoresis, separated proteins were transferred to low fluorescence PVDF membranes and blocked with PBS-T (PBS plus 0.1% Tween 20) and 5% of non-fat dry milk for 2 hours at room temperature. Membranes were washed 5x with PBS-T and incubated with primary antibodies diluted (1:500 or 1:1,000) in PBS-T and 5% BSA for 18 hours at 4°C under gentle agitation. After washing 5x with PBS-T membranes were incubated with horseradish peroxidase (HRP)-conjugated secondary antibodies (1:5,000) for 1 hour at room temperature. Clarity and Clarity Max Western ECL (Bio-Rad) was used to detect HRP signal using digital-based imaging system (Chemidoc, Bio-Rad). Images were further analyzed using Image Lab software (Bio-Rad). Total protein (Stain free gel technology) was used as Loading control.

Immunoblot analysis of secreted proteins

MSC were primed with pIC for 24 hours. After that, supernatant was collected and centrifuged at 3,000 g for 15 minutes to remove cells and cell debris. Supernatant was transferred to a new tube then stored at -80°C for further analysis. Lastly, MSC supernatant was thawed on ice, then 1 mL of ExoQuick-TC (SBI) was added per 5 mL of supernatant, and tubes remained upright overnight at 4°C. ExoQuick-TC/supernatant mixtures were centrifuged at 1,500 g for 30 minutes. The supernatant solution was aspirated and residual solution spun down by centrifugation at 1,500 g for 5 minutes. All traces of fluid were removed by aspiration without disturbing the precipitated pellet. Pellets were resuspended in RIPA lysis buffer (ThermoFisher) with protease inhibitor (Sigma-Aldrich). Protein quantification and expression in the lysates were performed as described in Immunoblot analysis section.

QUANTIFICATION AND STATISTICAL ANALYSIS

Statistical analysis was performed using GraphPad PrismV9.0 software (GraphPad Software). Numerical data are presented as mean \pm SEM unless otherwise stated. Multiple groups were analyzed by one-way ANOVA followed by Sidak's or Turkey's multiple comparisons test unless otherwise stated. For the analysis of cytokine data, logarithmic transformation was performed to normalize the data distribution before conducting ANOVA. Statistical significance was set at $p < 0.05$. Graphical abstract created with [Biorender.com](https://biorender.com).